Vietnam Journal of Marine Science and Technology; Vol. 20, No. 2; 2020: 155–172
DOI: https://doi.org/10.15625/1859-3097/20/2/15087
http://www.vjs.ac.vn/index.php/jmst

A numerical model for simulation of near-shore waves and wave induced currents using the depth-averaged non-hydrostatic shallow water equations with an improvement of wave energy dissipation

Phung Dang Hieu[1,*], Phan Ngoc Vinh[2]

[1]*Vietnam Institute of Seas and Islands, Hanoi, Vietnam*
[2]*Institute of Mechanics, VAST, Vietnam*
[*]E-mail: hieupd@visi.ac.vn/phunghieujp@gmail.com

Received: 4 September 2019; Accepted: 12 December 2019

Abstract
This study proposes a numerical model based on the depth-integrated non-hydrostatic shallow water equations with an improvement of wave breaking dissipation. Firstly, studies of parameter sensitivity were carried out using the proposed numerical model for simulation of wave breaking to understand the effects of the parameters of the breaking model on wave height distribution. The simulated results of wave height near the breaking point were very sensitive to the time duration parameter of wave breaking. The best value of the onset breaking parameter is around 0.3 for the non-hydrostatic shallow water model in the simulation of wave breaking. The numerical results agreed well with the published experimental data, which confirmed the applicability of the present model to the simulation of waves in near-shore areas.

Keywords: Waves in surf zone, non-hydrostatic shallow water model, wave breaking dissipation.

Citation: Phung Dang Hieu, Phan Ngoc Vinh, 2020. A numerical model for simulation of near-shore waves and wave induced currents using the depth-averaged non-hydrostatic shallow water equations with an improvement of wave energy dissipation. *Vietnam Journal of Marine Science and Technology*, *20*(2), 155–172.

INTRODUCTION

Water surface waves in the near-shore zone are very complicated and important for the sediment transportation as well as bathymetry changes in the near-shore areas. The accurate simulation of near-shore waves could result in a good chance to estimate well the amount of sediment transportation. So far, scientists have made effort to simulate waves in the near-shore areas for several decades. Conventionally, Navier-Stokes equations are accurate for the simulation of water waves in the near-shore areas including the complicated processes of wave propagation, shoaling, deformation, breaking and so on. However, for the practical purpose, the simulation of waves by a Navier-Stokes solver is too expensive and becomes impossible for the case of three dimensions with a real beach. To overcome these difficulties, the Boussinesq type equations (BTE) have been used alternatively by coastal engineering scientists for more than two decades. Many researchers have reported successful applications of BTE to the simulation of near-shore waves in practice. Some notable studies could be mentioned such as Deigaard (1989) [1], Schaffer et al. (1993) [2], Madsen et al., (1997) [3, 4], Zelt (1991) [5], Kennedy et al., (2000) [6], Chen et al., (1999) [7] and Fang and Liu (1999) [8].

Recently, the success in application of the depth-integrated non-hydrostatic shallow water equations (DNHSWE) to the simulation of wave propagation and deformation reported by researches has provided a new type of equations for practical choices of coastal engineers. DNHSWE derived from depth-integrating Navier-Stokes equations [9] contains non-hydrostatic pressure terms applicable to resolving the wave dispersion effect in simulation of short wave propagation. Compared to BTE which contains terms with high order spatial and temporal gradients, DNHSWE is relatively easy in numerical implementations as it contains only the first order gradient terms. These make DNHSWE become attractive to the community of coastal engineering researchers. So far, DNHSWE has been successfully applied to the simulation of wave processes in the near-shore areas in several studies. Some notable studies of wave propagation and wave breaking have been reported by Walter (2005) [10], Zijlema and Stelling (2008) [11], Yamazaki et al., (2009) [12], Smit et al., (2013) [13], Wei and Jia (2014) [14], and Lu and Xie (2016) [15]. The results given by the latter researchers confirm that DNHSWE is powerful and applicable to the simulation of wave propagation and deformation including wave-wave interaction, wave shoaling, refraction, diffraction with acceptable accuracy and comparable to the BTE. In these studies, the comparisons of wave height between the simulated results and the experimental data were mostly carried out for cases with non-breaking waves or long waves. Very few tests were made for the cases with wave breaking in the surf zone. Thus, it is very difficult to assess DNHSWE in terms of the practical use in the surf zone where the wave breaking is dominant. Recently, Smit et al., (2013) [13] have proposed an approximation method of a so-called HFA (Hydraulic Front Approximation) for the treatment of wave breaking. Following this method, the non-hydrostatic pressure is assumed to be eliminated at breaking cells, then DNHSWE model reduces to the nonlinear shallow water model with some added terms accounting for the turbulent dispersion of momentum. Somewhat similarly to the technique given by Kennedy et al., (2000) [6], the onset of wave breaking based on the surface steep limitation is chosen. Notable discussion from Smit et al., (2013) [13] shows that the 3D version of non-hydrostatic shallow water model needs a vertical resolution of around 20 layers to get accurate solution of wave height as good as that simulated by DNHSWE model with HFA treatment. Thus, by adding a suitable term accounting for wave breaking energy dissipation to DNHSWE, DNHSWE model becomes very powerful and applicable to a practical scale in the simulation of waves in the near-shore areas. The simulated results given by Smit et al., (2013) [13] showed good agreements with the experimental data given by Ting and Kirby (1994) [16]. The 3D version of non-hydrostatic shallow water model is very accurate in the simulation of

wave dynamics in surf zones. However, it is still very time consuming for the simulation of a practical case.

The objective of the present study is to introduce another method with dissipation terms for DNHSWE to account for the wave energy dissipation due to wave breaking. Numerical tests are conducted to estimate the effects of the dissipation terms on the simulation of waves in near-shore areas including wave breaking in surf zones. Comparisons between the simulated results and the experimental data are also carried out to examine the effectiveness of the model. Results of the present study reveal that DNHSWE model including the dissipation terms can be applicable to the simulation of waves in near-shore areas with an acceptable accuracy.

NUMERICAL MODEL

Governing equations

Following the derivation given by Yamazaki et al., (2009) [12], the depth-integrated non-hydrostatic shallow water equations can be written as follows:

The momentum conservation equations for the depth-averaged flow in the x and y direction:

$$\frac{\partial U}{\partial t}+U\frac{\partial U}{\partial x}+V\frac{\partial U}{\partial y}=-g\frac{\partial \zeta}{\partial x}-\frac{1}{2\rho}\frac{\partial q}{\partial x}-\frac{q}{2\rho D}\frac{\partial(\zeta-h)}{\partial x}-n^2\frac{g}{D^{1/3}}\frac{U\sqrt{U^2+V^2}}{\rho D} \quad (1)$$

$$\frac{\partial V}{\partial t}+U\frac{\partial V}{\partial x}+V\frac{\partial V}{\partial y}=-g\frac{\partial \zeta}{\partial y}-\frac{1}{2\rho}\frac{\partial q}{\partial y}-\frac{q}{2\rho D}\frac{\partial(\zeta-h)}{\partial y}-n^2\frac{g}{D^{1/3}}\frac{V\sqrt{U^2+V^2}}{\rho D} \quad (2)$$

The momentum conservation equation for the vertical depth-averaged flow:

$$\frac{\partial W}{\partial t}=\frac{q}{\rho D} \quad (3)$$

The conservation of mass equation for mean flow:

$$\frac{\partial \zeta}{\partial t}+\frac{\partial(UD)}{\partial x}+\frac{\partial(VD)}{\partial y}=0 \quad (4)$$

Boundary equations at the free surface and at the bottom are as follows:

$$w_s=\frac{d(\zeta)}{dt}=\frac{\partial \zeta}{\partial t}+u\frac{\partial \zeta}{\partial x}+v\frac{\partial \zeta}{\partial y} \text{ at } z=\zeta \quad (5)$$

$$w_b=\frac{d(-h)}{dt}=-u\frac{\partial h}{\partial x}-v\frac{\partial h}{\partial y} \text{ at } z=-h \quad (6)$$

Where: (U, V, W) are the velocity components of the depth-averaged flow in the x, y, z directions, respectively; q is the non-hydrostatic pressure at the bottom; n is the Manning coefficient; $\zeta = \zeta(x, y, t)$ is the displacement of the free surface from the still water level; t is the time; ρ is the density of water; g is the gravitational acceleration; D is the water depth = $(h+\zeta)$.

Wave breaking approximation

Previous studies presented by Yamazaki et al., (2009) [12] showed that the governing equations for mean flows presented in section Governing equations were very good for the simulation of long waves and the propagation of non-breaking waves. However, these equations are not suitable enough for the simulation of water waves in coastal zones, where the waves are dominant with wave breaking phenomena. The reason is that the governing equations (1), (2) and (3) do not contain any terms accounting for the wave energy dissipation due to wave breaking. In order to apply the depth-integrated non-hydrostatic shallow water equations to the simulation of water waves in the near-shore areas, the treatment for wave energy dissipation due to wave breaking is needed.

So far, the wave energy dissipation methods have been derived for studying waves in shallow water with the application of Boussinesq equations. The successful studies can be mentioned such as those given by Madsen et al., (1997) [3, 4] and Kennedy et al.,

(2000) [6], which presented the results in very good agreement with experimental data for wave breaking in surf zones. In the present study, the method given by Kennedy et al., (2000) [6] is used, and then it is applied to the depth-integrated non-hydrostatic shallow water equations for water wave propagation in the near-shore areas.

Similarly to the method given by Kennedy et al., (2000) [6], in order to simulate the diffusion of momentum due to the surface roller of wave breaking, the terms R_{bx}, R_{by} and R_{bz} added to the right hand side of the momentum equations in the x, y, and z directions (Eqs. (1), (2) and (3)) are as follows:

$$R_{bx} = \frac{1}{h+\zeta}\left[\left(\frac{\partial}{\partial x}\nu_e \frac{\partial}{\partial x}(h+\zeta)U\right) + \frac{1}{2}\left(\frac{\partial}{\partial y}\nu_e \frac{\partial}{\partial y}(h+\zeta)U + \frac{\partial}{\partial y}\nu_e \frac{\partial}{\partial x}(h+\zeta)V\right)\right] \quad (7)$$

$$R_{by} = \frac{1}{h+\zeta}\left[\left(\frac{\partial}{\partial y}\nu_e \frac{\partial}{\partial y}(h+\zeta)V\right) + \frac{1}{2}\left(\frac{\partial}{\partial x}\nu_e \frac{\partial}{\partial y}(h+\zeta)U + \frac{\partial}{\partial x}\nu_e \frac{\partial}{\partial x}(h+\zeta)V\right)\right] \quad (8)$$

$$R_{bz} = \nu_e\left(\frac{\partial^2 W}{\partial x^2} + \frac{\partial^2 W}{\partial y^2}\right) \quad (9)$$

However, the terms in Eqs. (7), (8) and (9) only account for the horizontal momentum exchanges due to wave breaking. Thus, in order to account for the energy lost due to the breaking process (dissipation due to bottom friction, heat transfer, release to the air, sound, and so on) we introduce other dissipation terms associated with the dissipation of vertical velocity and non-hydrostatic pressure where wave breaking occurs as follows:

$$q = q^o - B\beta q^o \quad (10)$$

$$w_s = w_s^o - B\beta w_s^o \quad (11)$$

Where: q^o and w_s^o are the values of q and w_s at the previous time step, respectively; v_e is the turbulence eddy viscosity coefficient defined by Kennedy et al., (2000) [12]:

$$\nu_e = B\delta^2(h+\zeta)\frac{\partial \zeta}{\partial t} \quad (12)$$

$$B = \begin{cases} 1 & \zeta_t \geq 2\zeta_t^* \\ \dfrac{\zeta_t}{\zeta_t^*} - 1 & \zeta_t^* < \zeta_t < 2\zeta_t^* \\ 0 & \zeta_t \leq \zeta_t^* \end{cases} \quad (13)$$

$$\zeta_t^* = \begin{cases} \zeta_t^{(F)} & t \geq T^* \\ \zeta_t^{(I)} + \dfrac{t-t_0}{T^*}\left(\zeta_t^{(F)} - \zeta_t^{(I)}\right) & 0 \leq t - t_0 \leq T^* \end{cases} \quad (14)$$

With δ = 0.0–1.5, $T^* = \gamma\sqrt{h/g}$, $\zeta_t^{(I)} = \alpha\sqrt{gh}$, $\zeta_t^{(F)} = 0.15\sqrt{gh}$.

Where: T^* is the transition time (or duration of wave breaking event); t_0 is the time when wave breaking occurs, $t - t_0$ is the age of the breaking event; $\zeta_t^{(I)} = \alpha\sqrt{gh}$ is the initial onset of wave breaking (the value of parameter α varies from 0.35 to 0.65 according to Kennedy et al., (2000) [6]; $\zeta_t^{(F)}$ is the final value of wave breaking.

As wave breaking appears, the vertical movement velocity at the surface and non-hydrostatic pressure are assumed to be dissipated gradually in the forms of Eqs. (10), (11) for the breaking point and neighbor points during the breaking time T^*. Thus, there are two parameters affecting the dissipating process and these parameters are γ and β.

Numerical methods

In order to solve numerically the governing equations from (1) to (4) with boundary equations (5) and (6) including wave breaking approximation (7), (8), (9), (10) and (11), we employed a conservative finite difference scheme using the upwind flux approximation given by Yamazaki et al., (2009) [12]. The space staggered grid is used. The horizontal velocity components *U* and *V* are located at the cell interface. The free surface elevation ζ, the non-hydrostatic pressure *q*, vertical velocity and water depth are located at the cell center. The solution is decomposed into 3 phases: The hydrostatic phase, non-hydrostatic phase and breaking dissipation phase. The hydrostatic phase gives the intermediate solution with the contribution of hydrostatic pressure. Then, the intermediate values are used to find the solution of the non-hydrostatic pressure in the non-hydrostatic phase. In the last phase, the velocities of the motion are corrected using the non-hydrostatic pressure *q* and dissipation terms due to wave breaking to obtain the values at the new time step and then the free surface is determined using the corrected velocities.

Hydrostatic phase

For the horizontal momentum equations:

The horizontal momentum equations (1), (2) are discretized as follows:

$$\tilde{U}_{j,k}^{m+1} = U_{j,k}^{m} - \frac{g\Delta t}{\Delta x}\left(\zeta_{j,k}^{m} - \zeta_{j-1,k}^{m}\right) - \frac{\Delta t}{\Delta x}U_{p}^{m}\left(U_{j,k}^{m} - U_{j-1,k}^{m}\right) - \frac{\Delta t}{\Delta x}U_{n}^{m}\left(U_{j+1,k}^{m} - U_{j,k}^{m}\right)$$
$$- \frac{\Delta t}{\Delta y}\bar{V}_{xp}^{m}\left(U_{j,k}^{m} - U_{j,k-1}^{m}\right) - \frac{\Delta t}{\Delta y}\bar{V}_{xn}^{m}\left(U_{j,k+1}^{m} - U_{j,k}^{m}\right) - n^{2}g\frac{\Delta t U_{j,k}^{m}\sqrt{\left(U_{j,k}^{m}\right)^{2} + \left(\bar{V}_{xj,k}^{m}\right)^{2}}}{\left(D_{j-1,k}^{m} + D_{j,k}^{m}\right)^{4/3}} \quad (15)$$

$$\tilde{V}_{j,k}^{m+1} = V_{j,k}^{m} - \frac{g\Delta t}{\Delta y}\left(\zeta_{j,k+1}^{m} - \zeta_{j,k}^{m}\right) - \frac{\Delta t}{\Delta x}\bar{U}_{yp}^{m}\left(V_{j,k}^{m} - V_{j-1,k}^{m}\right) - \frac{\Delta t}{\Delta x}\bar{U}_{yn}^{m}\left(V_{j+1,k}^{m} - V_{j,k}^{m}\right)$$
$$- \frac{\Delta t}{\Delta y}V_{p}^{m}\left(V_{j,k}^{m} - V_{j,k-1}^{m}\right) - \frac{\Delta t}{\Delta y}V_{n}^{m}\left(V_{j,k+1}^{m} - V_{j,k}^{m}\right) - n^{2}g\frac{\Delta t V_{j,k}^{m}\sqrt{\left(\bar{U}_{yj,k}^{m}\right)^{2} + \left(V_{j,k}^{m}\right)^{2}}}{\left(D_{j,k}^{m} + D_{j,k+1}^{m}\right)^{4/3}} \quad (16)$$

Where: $\bar{V}_{xp}^{m}$, $\bar{V}_{xn}^{m}$, $\bar{U}_{yp}^{m}$, $\bar{U}_{yn}^{m}$ are the averaged advection speeds and defined in the form of Eqs. (17), (18) as follows:

$$\bar{U}_{yj,k}^{m} = \tfrac{1}{4}\left(U_{j,k}^{m} + U_{j+1,k}^{m} + U_{j+1,k+1}^{m} + U_{j,k+1}^{m}\right) \quad (17)$$

$$\bar{V}_{xj,k}^{m} = \tfrac{1}{4}\left(V_{j,k}^{m} + V_{j-1,k}^{m} + V_{j-1,k-1}^{m} + V_{j,k-1}^{m}\right) \quad (18)$$

The momentum advection speeds are determined by the method given by Yamazaki et al., (2009) [12] and used to estimate the velocities at the cell side and conservative upwind fluxes as follows:

For a positive flow:

$$U_{p}^{m} = \frac{\hat{U}_{pj,k}^{m} + \left|\hat{U}_{pj,k}^{m}\right|}{2}$$

and for a negative flow:

$$U_{n}^{m} = \frac{\hat{U}_{nj,k}^{m} - \left|\hat{U}_{nj,k}^{m}\right|}{2} \quad (19)$$

Where:

$$\hat{U}_{pj,k}^{m} = \frac{2FLU_{pj,k}^{m}}{D_{j-1,k}^{m} + D_{j,k}^{m}}, \hat{U}_{nj,k}^{m} = \frac{2FLU_{nj,k}^{m}}{D_{j-1,k}^{m} + D_{j,k}^{m}} \quad (20)$$

The numerical flux in the x direction for a positive flow $(U_{j,k}^m > 0)$ is estimated as follows:

$$FLU_{p\,j,k}^{\ m} = \begin{cases} \dfrac{U_{j-1,k}^m + U_{j-1,k}^m}{2}\left(h_{j-1,k} + \dfrac{\zeta_{j-2,k}^m + \zeta_{j-1,k}^m}{2}\right) & \text{for} \quad U_{j-1,k}^m > 0 \\ \dfrac{U_{j-1,k}^m + U_{j+1,k}^m}{2}\left(h_{j-1,k} + \zeta_{j-1,k}^m\right) & \text{for} \quad U_{j-1,k}^m \le 0 \end{cases} \tag{21}$$

and for a negative flow $(U_{j,k}^m < 0)$:

$$FLU_{n\,j,k}^{\ m} = \begin{cases} \dfrac{U_{j,k}^m + U_{j+1,k}^m}{2}\left(h_{j,k} + \dfrac{\zeta_{j,k}^m + \zeta_{j+1,k}^m}{2}\right) & \text{for} \quad U_{j+1,k}^m < 0 \\ \dfrac{U_{j,k}^m + U_{j+1,k}^m}{2}\left(h_{j,k} + \zeta_{j,k}^m\right) & \text{for} \quad U_{j+1,k}^m \ge 0 \end{cases} \tag{22}$$

Similarly, the momentum flux in the y direction is also estimated. The velocities V_p^m and V_n^m are defined as follows:

$$V_p^m = \frac{\hat{V}_{p\,j,k}^{\ m} + \left|\hat{V}_{p\,j,k}^{\ m}\right|}{2} \text{ for a positive flow and } V_n^m = \frac{\hat{V}_{n\,j,k}^{\ m} - \left|\hat{V}_{n\,j,k}^{\ m}\right|}{2} \text{ for a negative flow (23).}$$

Where: $\hat{V}_{pj,k}^{\ m} = \dfrac{2FLV_{p\,j,k}^{\ m}}{D_{j,k}^m + D_{j,k+1}^m}, \hat{V}_{nj,k}^{\ m} = \dfrac{2FLV_{n\,j,k}^{\ m}}{D_{j,k}^m + D_{j,k+1}^m}$ (24)

The numerical flux for a positive flow $(V_{j,k}^m > 0)$ is estimated as follows:

$$FLV_{p\,j,k}^{\ m} = \begin{cases} \dfrac{V_{j,k-1}^m + V_{j,k}^m}{2}\left(h_{j,k} + \dfrac{\zeta_{j,k-1}^m + \zeta_{j,k}^m}{2}\right) & \text{for} \quad V_{j,k-1}^m > 0 \\ \dfrac{V_{j,k-1}^m + V_{j,k}^m}{2}\left(h_{j,k} + \zeta_{j,k}^m\right) & \text{for} \quad V_{j,k-1}^m \le 0 \end{cases} \tag{25}$$

and for a negative flow $(U_{j,k}^m < 0)$:

$$FLV_{n\,j,k}^{\ m} = \begin{cases} \dfrac{V_{j,k}^m + V_{j,k+1}^m}{2}\left(h_{j,k+1} + \dfrac{\zeta_{j,k+1}^m + \zeta_{j,k+2}^m}{2}\right) & \text{for} \quad V_{j,k+1}^m < 0 \\ \dfrac{V_{j,k}^m + U_{j,k+1}^m}{2}\left(h_{j,k+1} + \zeta_{j,k+1}^m\right) & \text{for} \quad V_{j,k+1}^m \ge 0 \end{cases} \tag{26}$$

Note that the average velocity components: $\overline{U}_{y_p}^{\,m}$, $\overline{U}_{y_n}^{\,m}$, $\overline{V}_{x_p}^{\,m}$, $\overline{V}_{x_n}^{\,m}$ in Eqs. (15) and (16) are defined by Eqs. (17) and (18) with the values of $U_p^m, U_n^m, V_p^m, V_n^m$ estimated by equations from (19) to (26). The average values of $\zeta_{j,k}^m$ and $h_{j,k}$ are also determined by Eqs. (16), (17). Superscript *m* denotes the value at old time step.

For the mass conservation equation:

Eq. (4) is discretized as follows:

$$\zeta_{j,k}^{m+1} = \zeta_{j,k}^m - \Delta t \frac{FLX_{j+1,k} - FLX_{j,k}}{\Delta x} - \Delta t \frac{FLY_{j,k} - FLY_{j,k-1}}{\Delta y} \tag{27}$$

$$FLX_{j,k} = U_p^{m+1}\zeta_{j-1,k}^m + U_n^{m+1}\zeta_{j,k}^m + U_{j,k}^{m+1}\frac{h_{j-1,k} + h_{j,k}}{2} \tag{28a}$$

$$FLY_{j,k} = V_p^{m+1}\zeta_{j,k}^m + V_n^{m+1}\zeta_{j,k+1}^m + V_{j,k}^{m+1}\frac{h_{j,k} + h_{j,k+1}}{2} \tag{28b}$$

Where: $U_p^m = \dfrac{U_{j,k}^m + \left|U_{j,k}^m\right|}{2}$, $U_n^m = \dfrac{U_{j,k}^m - \left|U_{j,k}^m\right|}{2}$, $V_p^m = \dfrac{V_{j,k}^m + \left|V_{j,k}^m\right|}{2}$, $V_n^m = \dfrac{V_{j,k}^m - \left|V_{j,k}^m\right|}{2}$.

Non-hydrostatic phase

In this phase, the values at the new time step are determined from the intermediate values of velocity and non-hydrostatic pressure as follows:

$$U_{j,k}^{m+1} = \tilde{U}_{j,k}^{m+1} - \frac{\Delta t}{\rho \Delta x} A_{j,k} \frac{(q_{j,k}^{m+1} + q_{j-1,k}^{m+1})}{2} - \frac{\Delta t}{\rho \Delta x} \frac{(q_{j,k}^{m+1} - q_{j-1,k}^{m+1})}{2} \tag{29}$$

$$V_{j,k}^{m+1} = \tilde{V}_{j,k}^{m+1} - \frac{\Delta t}{\rho \Delta y} C_{j,k} \frac{(q_{j,k+1}^{m+1} + q_{j,k}^{m+1})}{2} - \frac{\Delta t}{\rho \Delta y} \frac{(q_{j,k+1}^{m+1} - q_{j,k}^{m+1})}{2} \tag{30}$$

Where: $A_{j,k} = \dfrac{(\zeta_{j,k}^m - h_{j,k}) - (\zeta_{j-1,k}^m - h_{j-1,k})}{D_{j,k}^m + D_{j-1,k}^m}$, $C_{j,k} = \dfrac{(\zeta_{j,k+1}^m - h_{j,k+1}) - (\zeta_{j,k}^m - h_{j,k})}{D_{j,k}^m + D_{j,k+1}^m}$ (31)

In order to find the values of $q_{j,k}^{m+1}$, the vertical momentum equation (3) is used and discretized as follows:

$$w_{s\,j,k}^{\,m+1} = w_{s\,j,k}^{\,m} - (w_{b\,j,k}^{\,m+1} - w_{b\,j,k}^{\,m}) + 2\frac{\Delta t}{\rho D_{j,k}^m} q_{j,k}^{m+1} \tag{32}$$

Where the approximation $W_{j,k} = \dfrac{1}{2}(w_{s\,j,k} + w_{b\,j,k})$ is assumed.

The vertical velocity component at the bottom is estimated using a finite difference upwind approximation for Eq. (6) as follows:

$$w_{b_{j,k}}^{m+1} = -\overline{U}_{z_p}^{m}\frac{h_{j,k}-h_{j-1,k}}{\Delta x} - \overline{U}_{z_n}^{m}\frac{h_{j+1,k}-h_{j,k}}{\Delta x} - \overline{V}_{z_p}^{m}\frac{h_{j,k}-h_{j,k-1}}{\Delta y} - \overline{V}_{z_n}^{m}\frac{h_{j,k+1}-h_{j,k}}{\Delta y} \tag{33}$$

Where:

$$\overline{U}_{z_p}^{m} = \frac{\overline{U}_{z_{j,k}}^{m} + \left|\overline{U}_{z_{j,k}}^{m}\right|}{2},\ \overline{U}_{z_n}^{m} = \frac{\overline{U}_{z_{j,k}}^{m} - \left|\overline{U}_{z_{j,k}}^{m}\right|}{2},\ \overline{V}_{z_p}^{m} = \frac{\overline{V}_{z_{j,k}}^{m} + \left|\overline{V}_{z_{j,k}}^{m}\right|}{2},\ \overline{V}_{z_n}^{m} = \frac{\overline{V}_{z_{j,k}}^{m} - \left|\overline{V}_{z_{j,k}}^{m}\right|}{2} \tag{34}$$

$$\overline{U}_{z_{j,k}}^{m} = \frac{U_{j,k}^{m} + U_{j+1,k}^{m}}{2},\ \overline{V}_{z_{j,k}}^{m} = \frac{V_{j,k}^{m} + V_{j,k-1}^{m}}{2} \tag{35}$$

Using the continuity equation with the approximation for one layer of water column, it can be written in the finite difference equation as follows:

$$\frac{U_{j+1,k}^{m+1} - U_{j,k}^{m+1}}{\Delta x} + \frac{V_{j,k}^{m+1} - V_{j,k-1}^{m+1}}{\Delta y} + \frac{w_{s_{j,k}}^{m+1} - w_{b_{j,k}}^{m+1}}{D_{j,k}^{m}} = 0 \tag{36}$$

Substituting the velocities at time step m+1 expressed through Eqs. (29), (30) and (32) into Eq. (36) yields the following Poisson equation for determining the non-hydrostatic pressure:

$$PL_{j,k}q_{j-1,k}^{m+1} + PR_{j,k}q_{j+1,k}^{m+1} + PB_{j,k}q_{j,k-1}^{m+1} + PT_{j,k}q_{j,k+1}^{m+1} + PC_{j,k}q_{j,k}^{m+1} = Q_{j,k} \tag{37}$$

Where:

$$\begin{aligned} A_{j,k} &= \frac{\left(\zeta_{j,k}^{m} - h_{j,k}\right) - \left(\zeta_{j-1,k}^{m} - h_{j-1,k}\right)}{\left(D_{j,k}^{m} + D_{j-1,k}^{m}\right)}, A_{j+1,k} = \frac{\left(\zeta_{j+1,k}^{m} - h_{j+1,k}\right) - \left(\zeta_{j,k}^{m} - h_{j,k}\right)}{\left(D_{j+1,k}^{m} + D_{j,k}^{m}\right)}, \\ C_{j,k} &= \frac{\left(\zeta_{j,k+1}^{m} - h_{j,k+1}\right) - \left(\zeta_{j,k}^{m} - h_{j,k}\right)}{\left(D_{j,k}^{m} + D_{j,k+1}^{m}\right)}, C_{j,k-1} = \frac{\left(\zeta_{j,k}^{m} - h_{j,k}\right) - \left(\zeta_{j,k-1}^{m} - h_{j,k-1}\right)}{\left(D_{j,k}^{m} + D_{j,k-1}^{m}\right)} \end{aligned} \tag{38}$$

$$\begin{aligned} PL_{j,k} &= \frac{\Delta t}{2\rho\Delta x^2}\left(-1 + A_{j,k}\right), PR_{j,k} = \frac{\Delta t}{2\rho\Delta x^2}\left(-1 - A_{j+1,k}\right), \\ PB_{j,k} &= \frac{\Delta t}{2\rho\Delta y^2}\left(-1 + C_{j,k-1}\right), PT_{j,k} = \frac{\Delta t}{2\rho\Delta y^2}\left(-1 - C_{j,k}\right) \end{aligned} \tag{39}$$

$$PC_{j,k} = \frac{\Delta t}{2\rho\Delta x^2}\left[\left(1 + A_{j,k}\right) + \left(1 - A_{j+1,k}\right)\right] + \frac{\Delta t}{2\rho\Delta y^2}\left[\left(1 + C_{j,k-1}\right) + \left(1 - C_{j,k}\right)\right] + \frac{2\Delta t}{\rho\left(D_{j,k}^{m}\right)^2} \tag{40}$$

$$Q_{j,k} = -\frac{\tilde{U}_{j+1,k}^{m+1} - \tilde{U}_{j,k}^{m+1}}{\Delta x} - \frac{\tilde{V}_{j,k}^{m+1} - \tilde{V}_{j,k-1}^{m+1}}{\Delta y} - \frac{w_{s\,j,k}^{m} + w_{b\,j,k}^{m} - 2w_{b\,j,k}^{m+1}}{D_{j,k}^{m}} \tag{41}$$

Equation (37) can be solved numerically to obtain the values of $q_{j,k}^{m+1}$. Then, the values of parameters B and v_e are determined by Eqs. (12) and (13). Values of R_{bx}, R_{by} and R_{bz} are determined by Eqs. (7), (8) and (9) using a central finite deference scheme for the second order derivatives.

Breaking dissipation phase

When wave breaking occurs, equation (10) is used to obtain the values of non-hydrostatic pressure $q^{*m+1}_{j,k}$ as follows:

$$q^{*m+1}_{j,k} = q^{m+1}_{j,k} - B\beta q^{m+1}_{j,k} \tag{42}$$

The corrections for velocity components of flow including effects of wave breaking are as follows:

$$U^{m+1}_{j,k} = \tilde{U}^{m+1}_{j,k} - \frac{\Delta t}{\rho \Delta x} A_{j,k} \frac{(q^{*m+1}_{j,k} + q^{*m+1}_{j-1,k})}{2} - \frac{\Delta t}{\rho \Delta x} \frac{(q^{*m+1}_{j,k} - q^{*m+1}_{j-1,k})}{2} + R_{bx}\Delta t \tag{43}$$

$$V^{m+1}_{j,k} = \tilde{V}^{m+1}_{j,k} - \frac{\Delta t}{\rho \Delta y} C_{j,k} \frac{(q^{*m+1}_{j,k+1} + q^{*m+1}_{j,k})}{2} - \frac{\Delta t}{\rho \Delta y} \frac{(q^{*m+1}_{j,k+1} - q^{*m+1}_{j,k})}{2} + R_{by}\Delta t \tag{44}$$

$$w^{m+1}_{s\,j,k} = w^{m}_{s\,j,k} - (w^{m+1}_{b\,j,k} - w^{m}_{b\,j,k}) + 2\frac{\Delta t}{\rho D^{m}_{j,k}} q^{*m+1}_{j,k} - B\beta w^{m}_{s\,j,k} + R_{bz}\Delta t \tag{45}$$

After determining the velocity components at the correction step, the conservation of mass equation is used for determination of the free surface elevation and the total water depth. Equation (27) is employed to determine values of $\zeta^{m+1}_{j,k}$ explicitly.

The computational procedure can be briefly described as follows:

Initials: The values of all variables are given at time step m as the initial condition:

1) Give values of variables at forcing boundaries;

2) Compute $\tilde{U}^{m+1}_{j,k}$, $\tilde{V}^{m+1}_{j,k}$ (Eqs. (15), (16)) using known variables at time step m;

3) Compute coefficients $A_{j,k}$, $C_{j,k}$, and $Q_{j,k}$ using known values of variables at time step m and $\tilde{U}^{m+1}_{j,k}$, $\tilde{V}^{m+1}_{j,k}$, for Poisson equation (Eqs. (38), (39), (40) and (41));

4) Solve Poisson Eq. (37) to get values of $q^{m+1}_{j,k}$ using BiCG-STAB method;

5) Compute the values of the breaking parameters using Eqs. (12)–(4);

6) Correct values of $q^{m+1}_{j,k}$ with breaking effects using (42) and then compute the values of $U^{m+1}_{j,k}$, $V^{m+1}_{j,k}$, $\omega^{m+1}_{s\,j,k}$ from Eqs. (43), (44) and (45);

7) Calculate the values of $\zeta^{m+1}_{j,k}$ by using Eq. (27);

8) The variables at the new time step m+1 are assigned to the values at old time step m. Return to step 1 and repeat steps from 1 to 8 for the next time step until the specified time.

Stability condition requires the time step Δt to satisfy the well-known CFL condition for propagation of long gravity waves and dispersion of viscous terms. In the present study, we choose $\Delta t = 0.25 \min\{\Delta x, \Delta y\} / \sqrt{g(h_{\max} + \zeta)}$ for all simulations.

Wet-dry boundary and wave maker source

For the treatment of run-up calculations, the interface between wet and dry cells is extrapolated following the approach of Kowalik et al., (2005) [17]. The numerical solutions are extrapolated from the wet region onto the beach. The non-hydrostatic pressure is set to be zero at the wet cells along the wet-dry interface. The moving waterline scheme

provides an update of the wet-dry interface as well as the associated flow depth and velocity at the beginning of every time step. A maker index $IDX_{j,k}^{m}$ is introduced to identify the computation region. First, the index $IDX_{j,k}^{m}$ is set based on the flow depth of the cell, $IDX_{j,k}^{m}=1$ if the flow depth is positive and $IDX_{j,k}^{m}=0$ if the flow depth is zero or negative. Then, the surface elevation along the interface determines any advancement of the waterline. For flows in the positive *x* direction, if $IDX_{j,k}^{m}=0$ and $IDX_{j-1,k}^{m}=1$ then cell index is re-evaluated as $IDX_{j,k}^{m}=1$ (wet) if $\zeta_{j-1,k}^{m}>-h_{j,k}$, $IDX_{j,k}^{m}=0$ (dry) if $\zeta_{j-1,k}^{m}\le -h_{j,k}$.

If a cell becomes wet, the flow depth and velocity components at the cell are set as:

$$D_{j,k}^{m}=\zeta_{j-1,k}^{m}+h_{j,k},\ U_{j,k}^{m}=U_{j-1,k}^{m}$$

The marker indexes are then updated for flows in the negative *x* direction. The same procedures are implemented in the *y* direction. For case the water flows into a new cell from multiple directions, the flow depth is averaged.

After completing the re-evaluation step of the marker indexes and variables, the computation is advanced for the next time step for the wet region. To avoid the numerical instability due to a cell frequently exchanged between dry and wet status, we used a small value of 10^{-5} m for a critical dry depth instead of using zero.

To generate surface waves for numerical experiments, the internal generation wave source method of Wei et al., (1999) [18] is adopted. In the method, there are two components accounting for the source function term and the sponge dissipation layer added to the momentum equation (refer to Wei et al., (1999) [18] for more detail).

SIMULATION RESULTS AND DISCUSSIONS

Wave breaking on a planar beach

The experimental data of wave breaking on a 1/35 slopping beach given by Ting and Kirby (1994) [16] was used to verify the capability of the proposed numerical model in the simulation of wave breaking in surf zone.

Simulation condition

The computational domain was similar to that in the experiment done by Ting and Kirby (1994) [16]. Fig. 1 presents the bathymetry of the domain with a 1/35 slopping beach and alongshore width of 1 m.

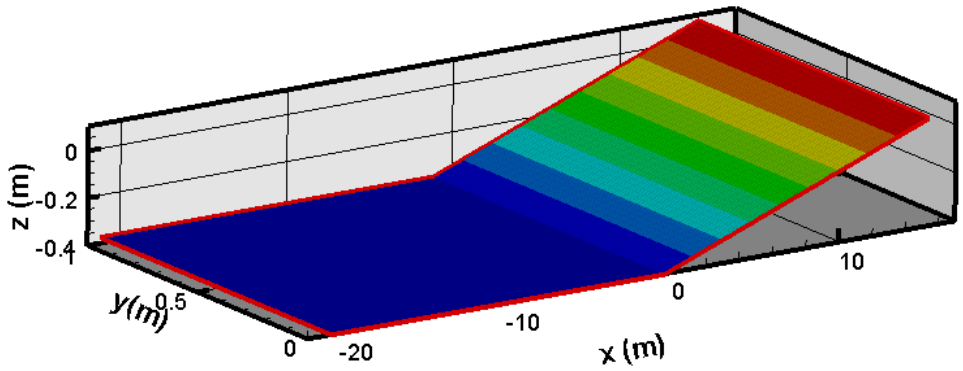

Figure 1. Bathymetry for simulation of waves on 1/35 slopping beach

Note that the simulation was carried out with 2D depth-integrated non-hydrostatic shallow water model instead of 1D model. Firstly, a study of parameter sensitivity was done in order to get appropriate values of the parameters of the numerical model. The incident wave condition for the numerical model is similar to that for the physical

experiment done by Ting and Kirby (1994) [16] (for case with the regular incident wave height and period of 0.125 m and 2.0 s, respectively). A regular orthogonal mesh with $\Delta x = \Delta y = 0.05$ m was used for all simulations.

Parameter sensitivity

Due to the modification of the wave breaking model, there are several parameters whose sensitivity needs inspecting to understand how and how much they affect the simulated results. These parameters include the onset wave breaking coefficient α, the duration of wave breaking coefficient γ (in the formula $T^* = \gamma\sqrt{h/g}$), and the dissipation percentage coefficient β. The final value of wave breaking $\zeta_t^{(F)}$ is not significantly sensitive to simulated wave heights, therefore, we use the fixed value $\zeta_t^{(F)} = 0.15\sqrt{gh}$ and δ = 1.5 as recommended by Kennedy et al., (2000) [6].

Kennedy et al., (2000) [6] suggested that the value of α ranges from 0.35 to 0.65. However, the simulated results of waves on the 1/35 slopping beach by the present model show that the value of α should be smaller than 0.35. Fig. 2 presents the effects of the onset breaking parameter α on the simulated wave height distribution in comparison with the experimental data given by Ting and Kirby (1994) [16]. It is clearly observed that the value of α equal to or greater than 0.35 makes the wave breaking location shift shoreward in comparison with the experimental data. The smaller value of α produces the earlier breaking effect. The best value of α is found around 0.3.

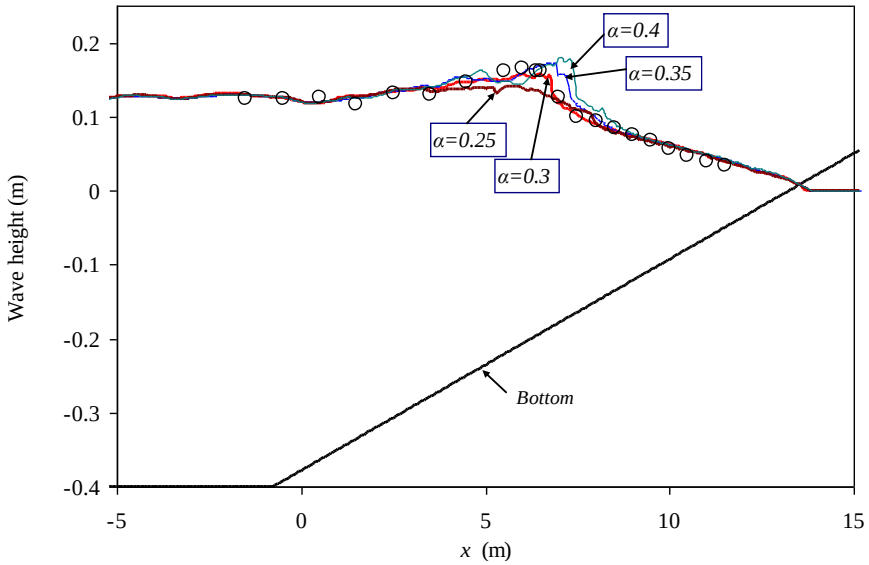

Figure 2. Influence of the onset breaking parameter α on simulated wave height distribution (Continuous lines: Simulated wave height; circles: experimental data [16])

Fig. 3 shows the influence of breaking duration parameter γ on the simulated wave height distribution. The following observations can be made from the figure: The value of γ = 5.0 suggested by Kennedy et al., (2000) [6] makes the underestimated energy dissipation then the wave height in the surf zone is overestimated; the smaller value of γ makes the greater dissipation effect near the breaking location; the wave height distribution near the breaking point is very sensitive to the value of γ. These mean that the duration of wave breaking in the present model is important to the simulation of waves in surf zone. The appropriate value of γ could be in the range from 0.4 to 0.6. Then we take γ = 0.55 for all of other simulations. γ = 0.55 and α = 0.31 are employed to investigate the

influence of the dissipation percentage coefficient β on the wave breaking simulation. The results are presented in fig. 4. It can be seen that the variation of β causes a change in wave height at the breaking point and in the surrounding area. The smaller value of β makes the smaller amount of wave energy dissipated after duration of breaking event $T^* = \gamma\sqrt{h/g}$. The value of β equal to or greater than 0.4 gives almost similar results of wave height distribution at the breaking point and others. Thus, in the present study from now on, β = 0.5 is chosen for all of other simulations. Fig. 5 presents comparison of mean water levels between the simulated results and experimental data. The simulated mean water levels agree well with experimental data in the distance from the breaking point toward offshore region. The setup region after the breaking point shoreward is clearly seen. However, there are some discrepancies from the experimental data.

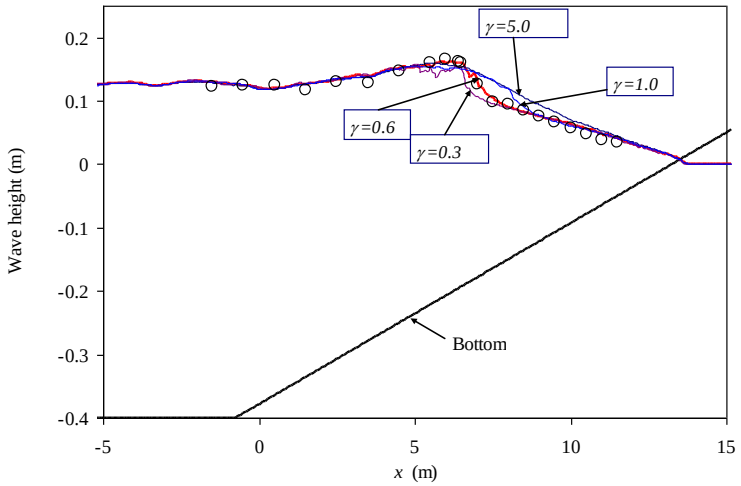

Figure 3. Influence of the breaking duration parameter γ on simulated wave height distribution (Continuous lines: Simulated wave height; circles: experimental data [16])

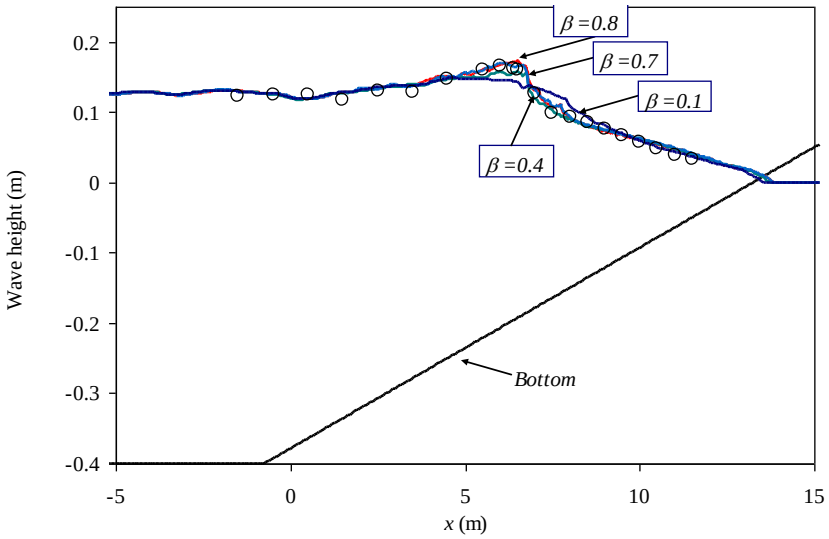

Figure 4. Influence of dissipation parameter β on simulated wave height distribution (Continuous lines: simulated wave height; circles: experimental data [16])

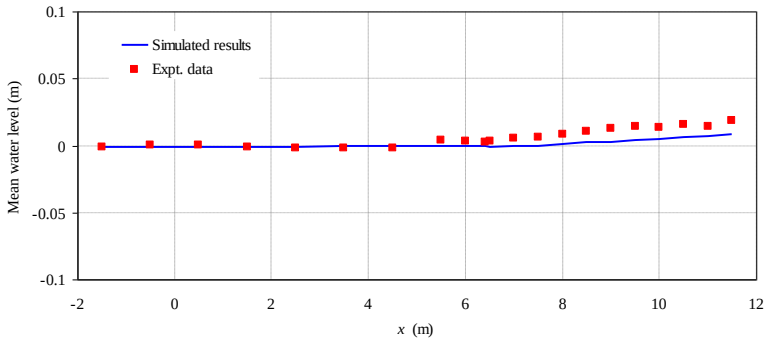

Figure 5. Comparison of mean water levels between simulated results and experimental data [16]

Wave induced current with a rip channel

Experimental condition and simulation setup

The experiment on near-shore wave propagation over a rip channel given by Hamm (1992) [19] is well-known in the coastal engineering community. For testing the present numerical model with the proposed method of wave breaking dissipation, the experimental data given by Hamm (1992) [19] were employed.

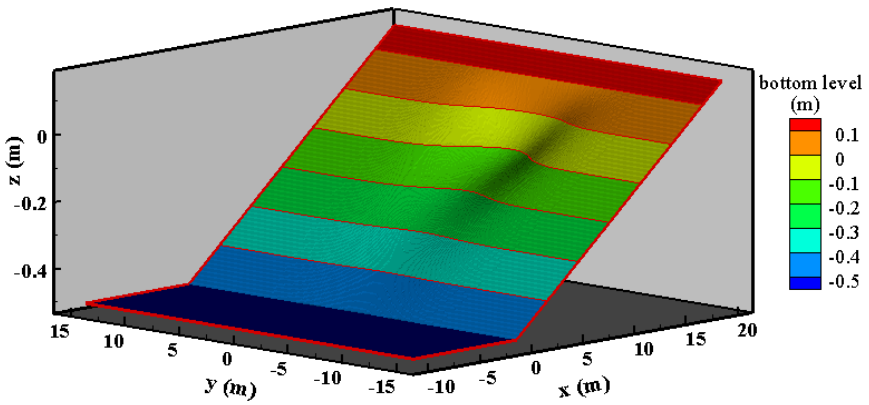

Figure 6. Bathymetry for numerical simulation similar to the experiment by Hamm (1992) [19]

The numerical simulation conditions were set up with the bathymetry and wave conditions similar to those in the experiment done by Hamm (1992) [19]. Numerical simulation was carried out for cases with unidirectional irregular waves with significant height of 0.13 m and peak period of 1.60 s. The experimental data of wave height distribution along the rip channel and on the cross-shore planar beach and the experimental data of the current distribution at rip channel were used for the comparison with numerical results. Fig. 6 shows the bathymetry of the computational domain. For the numerical simulation, both regular and irregular incident waves were imposed.

Results and discussion

Numerical simulation was carried out for 200 peak wave periods to get a quasi-steady state. The significant wave heights were determined by using the well-known formula $H_s = 4.004\sqrt{\sigma_\zeta^2}$ (where σ_ζ^2 is the variance of the water free surface elevation). The wave induced currents are determined by averaging the velocity at each cell in the duration of five peak wave periods.

Fig. 7 shows the distribution of the simulated significant wave height in the computational domain. Along two cross sections R-R at rip channel and B-B on the planar beach (see fig. 7), the simulated wave

height and velocity were extracted to be compared to the experimental data given by Hamm (1992) [19].

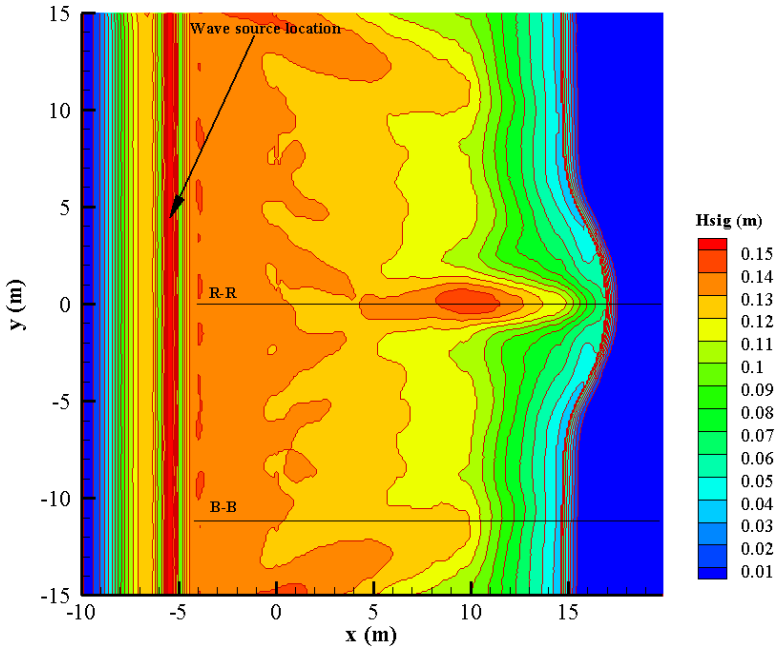

Figure 7. Distribution of significant wave height in the computational domain (case with incident waves: *Hs* = 0.13 m, *Tp* = 1.60 s, uniform direction)

Fig. 8 presents the comparison of wave height between the simulated and experimental results along the rip channel R-R and the cross-section B-B. The following observations can be made from fig. 8a: The simulated wave heights with regular and irregular incident waves are in good agreement with the experimental data; distribution of the simulated regular wave height agrees very well with experimental data, and agrees better than that of the simulated irregular incident waves; inside the surf zone, the simulated significant wave heights were slightly overestimated in comparison with the experimental data; the differences between the experimental and simulated wave heights reduce in the area close to shoreline; this gives a confidence in the simulation of run-up and wave induced currents using the present model. Along the section B-B, very good agreement is again obtained (see fig. 8b).

Comparisons of the module of velocity along the rip channel R-R are presented in Fig. 9. Good agreements between the simulated and the experimental results are clearly observed. Surprisingly, the simulated rip velocity with the regular incident wave is still in good agreement with the experimental data which were produced with irregular incident waves in the experiment done by Hamm (1992) [19]. However, the present model underestimated the maximum rip velocity.

The distribution of wave induced currents in the computational domain including rip currents is shown in fig. 10. Rip current and long shore currents are clearly observed in the figure. Water from both sides of the rip channel tends to converge to the rip channel and form an offshoreward current with the high velocity in the middle of the channel. Longshore currents near the shoreline can also be clearly observed. In the rip channel, waves were stopped by the inverted current from the shore, which makes the waves become steep and broken on the rip (see fig. 11). From fig. 11 the run-up of waves on the beach is clearly observed and the interaction of waves in the near-shore area for the simulation case is really complicated.

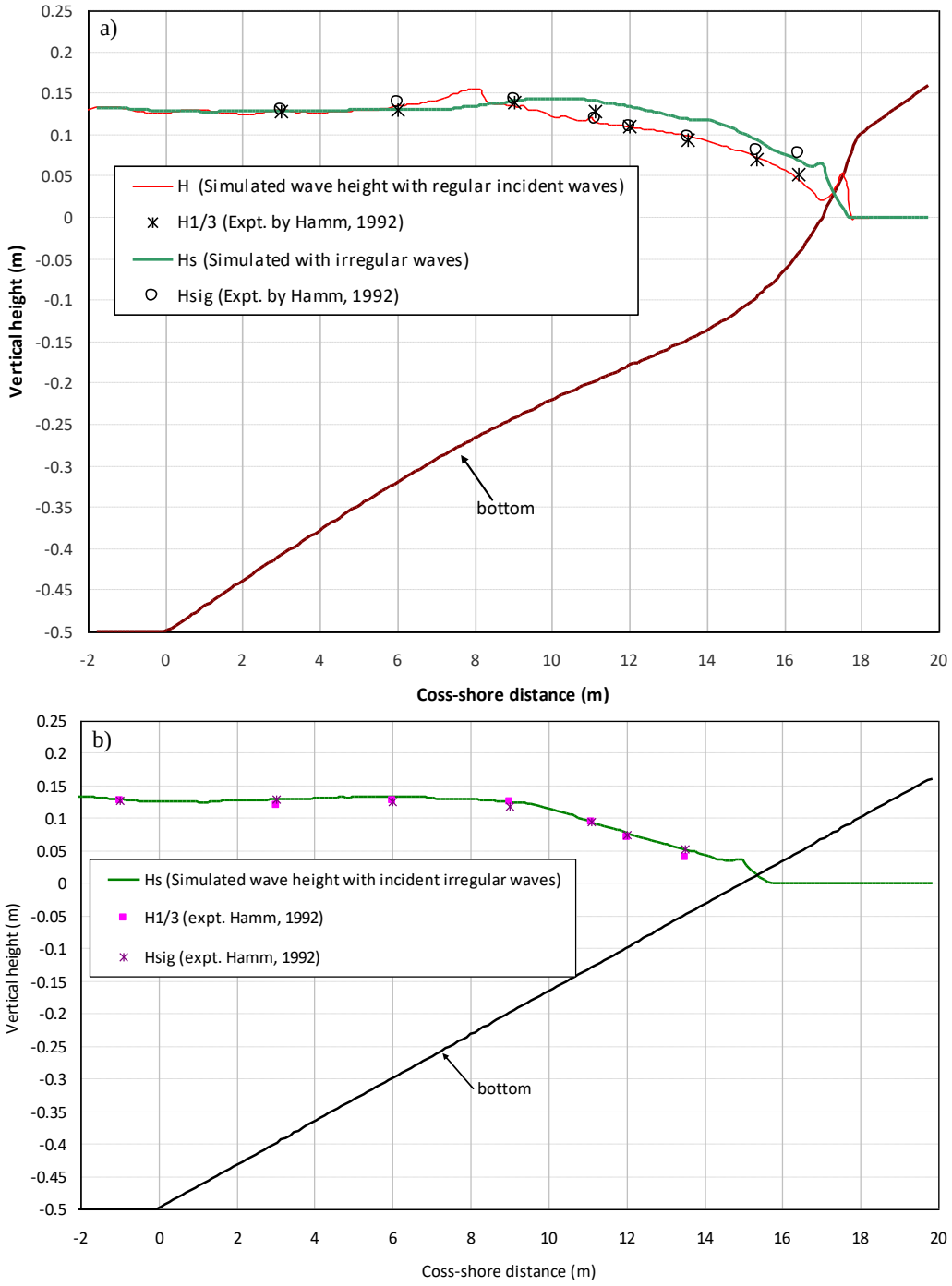

Figure 8. Distribution of wave height along: a) Rip channel R-R; b) Cross-section B-B on the plane beach (case with incident waves: *Hs* = 0.13 m, *Tp* = 1.60 s, uniform direction)

In brief, a series of the above-mentioned simulated results shows that the present model can simulate well wave propagation in the near-shore areas including effects of wave-current interaction, wave shoaling, wave breaking and wave-wave interaction with acceptable accuracy.

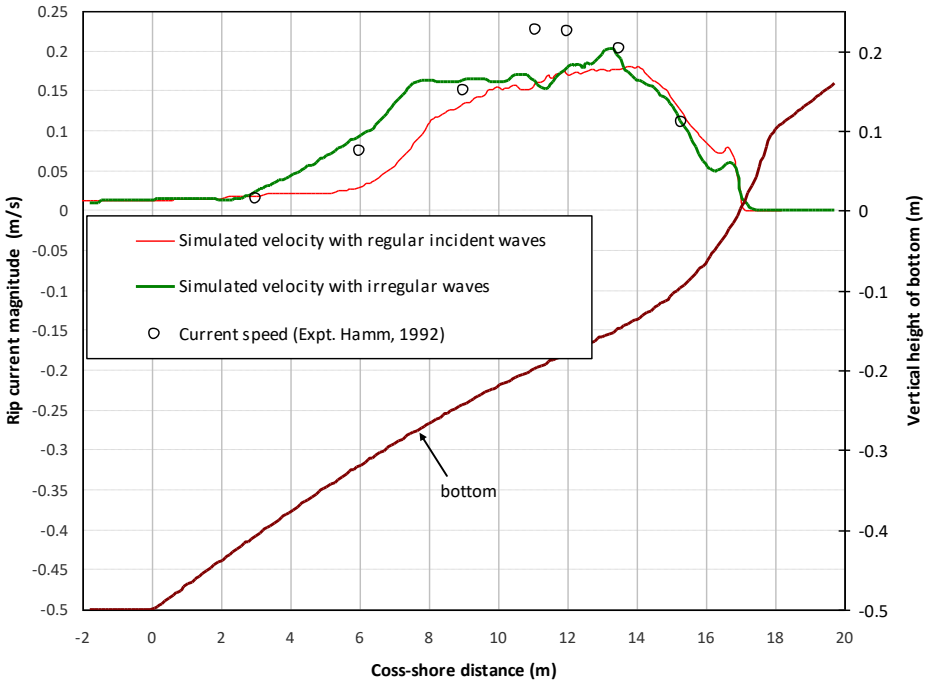

Figure 9. Distribution of wave induced rip current velocity along the rip channel (case with incident waves: *Hs* = 0.13 m, *Tp* = 1.60 s, uniform direction)

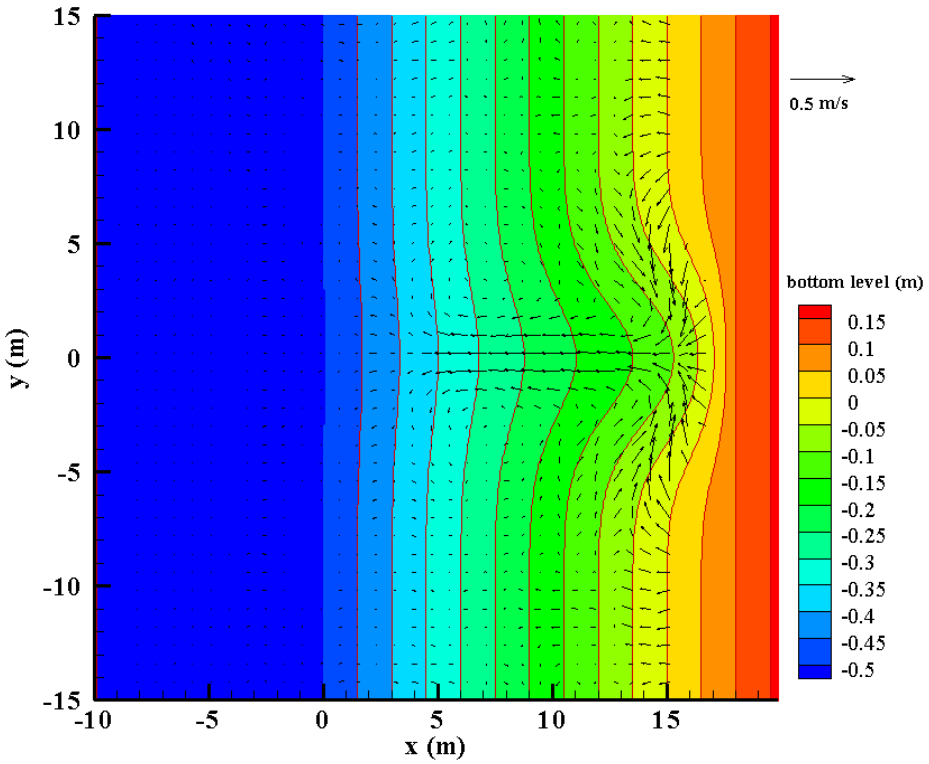

Figure 10. Distribution of wave induced currents in the computational domain (case with incident waves: *Hs* = 0.13 m, *Tp* = 1.60 s, uniform direction)

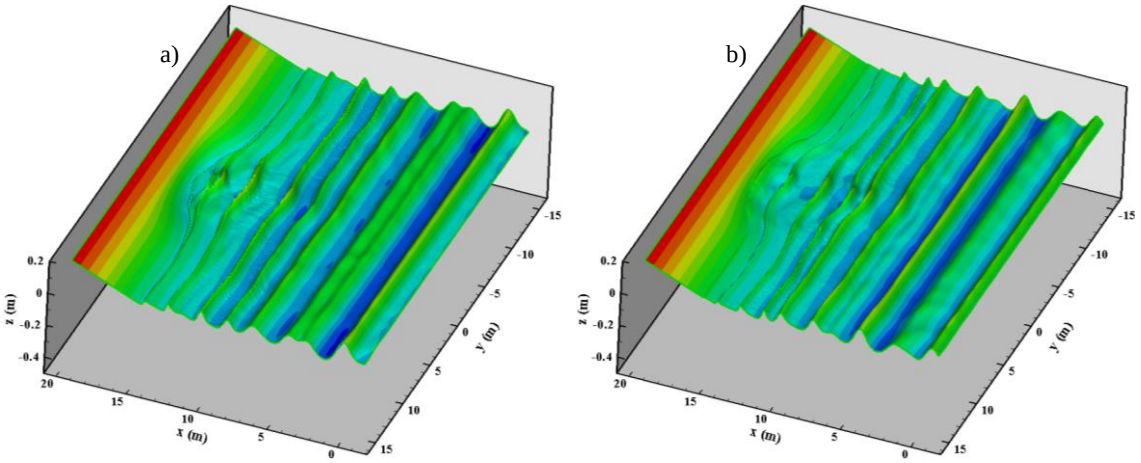

Figure 11. Snapshots of free surface due to irregular waves (case with incident waves: *Hs* = 0.13 m, *Tp* = 1.60 s, uniform direction)

CONCLUSIONS

The present study has proposed a numerical model based on the depth-integrated non-hydrostatic shallow water equations with an improvement of wave breaking dissipation using a modification of the method proposed by Kennedy et al., (2000) [6]. Firstly, numerical studies of the parameter sensitivity were carried out in order to understand the effects of the parameters on the simulated results of waves. It is found that with the present method, the simulated results of wave height near the breaking point are very sensitive to the time duration of wave breaking. The best value of the onset breaking parameter is around 0.3 for the present model. Then, the proposed numerical model was verified by some published experimental data.

Comparison between the simulated results and the experimental data confirmed that the present model is good for the simulation of waves in the near-shore areas. However, the model does not include the nonlinear shallow wave generation source method (such as the Cnoidal's waves); therefore, the model has not been verified for the case of plunging breaker. In the future, more verification of the model on wave plunging breaker needs to be carried out and consideration for improving simulation of wave setup is left for further study.

The present model has been successfully applied to the simulation of regular and irregular waves. However, further verification of the model needs to be carried out with the field observation data to confirm applicability of the model to real cases.

Acknowledgements: This work has been done under the financial support of Vietnam's National Foundation for Science and Technology Development (NAFOSTED) by the project grant number 105.06-2016.01. The financial support from NASFOSTED is gratefully acknowledged. The first author wishes to give thanks to Vietnam Institute of Sea and Islands (VISI) for providing good condition for the research. Lastly, the first author would like to send special thanks to Prof. Kirby J. T. and Dr. Ting F. C. K. for kindly providing the experimental data.

REFERENCES

[1] Deigaard, R., 1989. Mathematical modelling of waves in the surf zone. *Prog. Rep*, *69*, 47–59.

[2] Schäffer, H. A., Madsen, P. A., and Deigaard, R., 1993. A Boussinesq model for waves breaking in shallow water. *Coastal Engineering*, *20*(3–4), 185–202.

[3] Madsen, P. A., Sørensen, O. R., and Schäffer, H. A., 1997. Surf zone dynamics simulated by a Boussinesq type model. Part I. Model description and cross-shore motion of regular waves. *Coastal Engineering*, *32*(4), 255–287.

[4] Madsen, P. A., Sørensen, O. R., and Schäffer, H. A., 1997. Surf zone dynamics simulated by a Boussinesq type model. Part II: Surf beat and swash oscillations for wave groups and irregular waves. *Coastal Engineering*, *32*(4), 289–319.

[5] Zelt, J. A., 1991. The run-up of nonbreaking and breaking solitary waves. *Coastal Engineering*, *15*(3), 205–246.

[6] Kennedy, A. B., Chen, Q., Kirby, J. T., and Dalrymple, R. A., 2000. Boussinesq modeling of wave transformation, breaking, and runup. I: 1D. *Journal of Waterway, Port, Coastal, and Ocean Engineering*, *126*(1), 39–47.

[7] Chen, Q., Dalrymple, R. A., Kirby, J. T., Kennedy, A. B., and Haller, M. C., 1999. Boussinesq modeling of a rip current system. *Journal of Geophysical Research: Oceans*, *104*(C9), 20617–20637.

[8] Fang, K., and Liu, Z., 1999. Modeling Breaking Waves and Wave-induced Currents with Fully Nonlinear Boussinesq Equations. *WSEAS Transactions on Fluid Mechanics*, *9*, 131–143.

[9] Stelling, G., and Zijlema, M., 2003. An accurate and efficient finite-difference algorithm for non-hydrostatic free-surface flow with application to wave propagation. *International Journal for Numerical Methods in Fluids*, *43*(1), 1–23.

[10] Walters, R. A., 2005. A semi-implicit finite element model for non-hydrostatic (dispersive) surface waves. *International Journal for Numerical Methods in Fluids*, *49*(7), 721–737.

[11] Zijlema, M., and Stelling, G. S., 2008. Efficient computation of surf zone waves using the nonlinear shallow water equations with non-hydrostatic pressure. *Coastal Engineering*, *55*(10), 780–790.

[12] Yamazaki, Y., Kowalik, Z., and Cheung, K. F., 2009. Depth-integrated, non-hydrostatic model for wave breaking and run-up. *International Journal for Numerical Methods in Fluids*, *61*(5), 473–497.

[13] Smit, P., Zijlema, M., and Stelling, G., 2013. Depth-induced wave breaking in a non-hydrostatic, near-shore wave model. *Coastal Engineering*, *76*, 1–16.

[14] Wei, Z., and Jia, Y., 2014. Simulation of nearshore wave processes by a depth-integrated non-hydrostatic finite element model. *Coastal engineering*, *83*, 93–107.

[15] Lu, X., and Xie, S., 2016. Depth-averaged non-hydrostatic numerical modeling of nearshore wave propagations based on the FORCE scheme. *Coastal Engineering*, *114*, 208–219.

[16] Ting, F. C., and Kirby, J. T., 1994. Observation of undertow and turbulence in a laboratory surf zone. *Coastal Engineering*, *24*(1–2), 51–80.

[17] Kowalik, Z., Knight, W., Logan, T., and Whitmore, P., 2005. Numerical modeling of the global tsunami: Indonesian tsunami of 26 December 2004. *Science of Tsunami Hazards*, *23*(1), 40–56.

[18] Wei, G., Kirby, J. T., and Sinha, A., 1999. Generation of waves in Boussinesq models using a source function method. *Coastal Engineering*, *36*(4), 271–299.

[19] Hamm, L., 1993. Directional nearshore wave propagation over a rip channel: an experiment. In *Coastal Engineering 1992* (pp. 226–239).